

pubs.acs.org/cm Article

A Low-Temperature Growth Mechanism for Chalcogenide Perovskites

Ruiquan Yang, Jessica Nelson, Calvin Fai, Hasan Arif Yetkin, Chase Werner, Merielle Tervil, Alexander D. Jess, Phillip J. Dale, and Charles J. Hages*



Cite This: https://doi.org/10.1021/acs.chemmater.3c00494



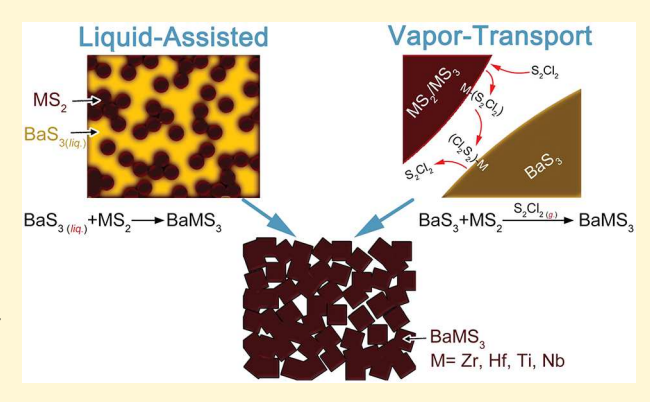
ACCESS I

III Metrics & More

Article Recommendations

s Supporting Information

ABSTRACT: Chalcogenide perovskites have attracted increasing research attention in recent years due to their promise of unique optoelectronic properties combined with stability. However, the synthesis and processing of these materials has been constrained by the need for high temperatures and/or long reaction times. In this work, we address the open question of a low-temperature growth mechanism for BaZrS₃. Ultimately, a liquid-assisted growth mechanism for BaZrS₃ using molten BaS₃ as a flux is demonstrated at temperatures $\geq 540~^{\circ}\text{C}$ in as little as 5 min. The role of Zr-precursor reactivity and S_(g.) on the growth mechanism and the formation of Ba₃Zr₂S₇ is discussed, in addition to the purification of resulting products using a straightforward H₂O wash. The extension of this growth mechanism to other Ba-based chalcogenides is shown, including BaHfS₃, BaNbS₃, and BaTiS₃. In addition, an alternative



vapor-transport growth mechanism is presented using S_2Cl_2 for the growth of BaZrS₃ at temperatures as low as 500 °C in at least 3 h. These results demonstrate the feasibility of scalable processing for the formation of chalcogenide perovskite thin-films.

1. INTRODUCTION

Chalcogenide perovskites have gained recent research attention due to their potential as Pb-free, inorganic perovskite semiconductors. Compared to hybrid halide perovskites, such as CH₃NH₃PbI₃, these chalcogenide perovskites have significantly improved structural stability. Compared to oxide perovskites, the inclusion of S or Se as anions reduces the band gap for applications with visible and NIR light. BaZrS₃ in particular has been a primary focus in recent research, possessing promising optoelectronic properties (primarily identified from theory) including band gap values relevant for photovoltaics, an extraordinarily high absorption coefficient, tolerance to deep defects, strong dielectric screening, favorable phonon properties, and desirable (isotropic) electron mobility for efficient charge transport. Additionally, BaZrS₃ is comprised of nontoxic and earth-abundant constituents.

However, the majority of reported syntheses require high temperatures and/or long reaction times. ^{4,5} Such reactions have kinetic limitations—for example, due to solid-state growth techniques—and/or thermodynamic limitations—for example, using highly stable oxide precursors. BaZrS₃ powders were reported as early as 1957 by Hahn and Mutschke¹⁰ via annealing of binary sulfides (BaS, ZrS₂) at 900 °C for 2 weeks. Alternatively, Clearfield¹¹ reported the reaction of BaZrO₃ with CS₂ at 950–1200 °C in 1963. Similar reactions were reported over the following 60 years using mixtures of BaS, ZrS₂,

BaCO₃, ZrO₂, and BaZrO₃. Recent progress in the synthesis of BaZrS₃ thin films is summarized in the following reactions. Márquez et al.¹² and Wei et al.¹³ formed BaZrS₃ via pulsed laser deposition (PLD) using a Ba-Zr-O target followed by annealing in a reactive sulfur species at ca. 800-1050 °C. Alternatively, Yu et al. 14 used a Ba-Zr-S target in PLD followed by an anneal with CS2 at 900 °C, and Surendran et al. 15 grew an expitaxial thin film of BaZrS₃ from a BaZrS₃ target using PLD in an H₂S environment at 700-850 °C. Comparotto et al. 16 formed BaZrS3 via cosputtering of Ba-Zr-S followed by sulfur-annealing from 650-900 °C. Sadeghi et al.¹⁷ reported BaZrS₃ grown via molecular beam epitaxy (MBE) at 900 °C. Gupta et al. 18 reported BaZrS₃ via sulfurization of BaZrO₃ at 1050 °C. While high-quality films were obtained in all these reports, oxidation is commonly reported and many of the methods require specialized equipment. Practical fabrication of BaZrS3 and other chalcogenide perovskites will require more moderate fabrication temperatures and shorter reaction times for cost-effective

Received: March 2, 2023 Revised: May 17, 2023



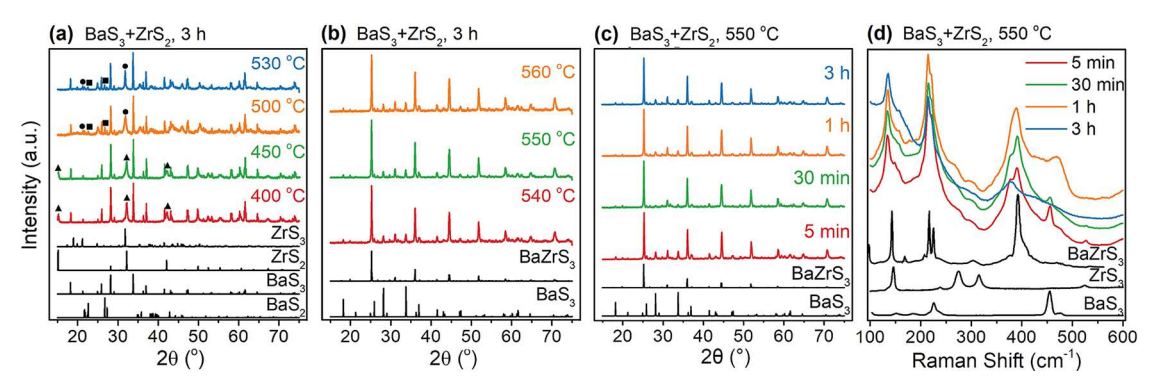


Figure 1. XRD patterns of samples from BaS₃ + ZrS₂ reactions (a) for 3 h at 400 °C, 450 °C, 500 °C, and 530 °C (triangles label ZrS₂, circles label for ZrS₃, and rectangles label BaS₂); (b) for 3 h at 540 °C, 550 °C, and 560 °C; and (c) at 550 °C for 5 min, 30 min, 1 h, and 3 h. (d) Raman spectra of samples from the reaction times in (c). Reference XRD patterns are shown in black labeled by compound (BaS₂ PDF 01-071-0377, BaS₃ PDF 01-073-1177, ZrS₂ PDF 01-089-4822, ZrS₃ PDF 01-080-0926, BaZrS₃ PDF 01-073-0847). Reference Raman spectrum for BaZrS₃ is from Gross et al. (measured at 14 K), ¹⁹ while ZrS₃ and BaS₃ are measured on our synthesized precursors (see SI).

manufacturing and the use of traditional substrates, such as glass.

Preparation of BaZrS₃ at lower temperatures has drawn recent attention, though this research is still at an early stage. We recently reported the synthesis of BaZrS₃ nanoparticles at 330 °C, ²⁰ with similar results reported by Zilevu at al. ²¹ Such nanoparticles are yet to be processed into device-grade films. Turnley et al.²² reported the solution-based synthesis of BaZrS₃ via sulfurization of an organometallic Ba precursor and ZrH₂ at temperatures above 550 °C; however, continuous, dense films were not possible in this approach. While these experiments demonstrate the ability for BaZrS3 to form at moderate temperatures, little is known about the lowtemperature growth mechanism. For instance, Wang et al.²³ reported a reaction for BaZrS₃ powders at 600 °C (7 days) using very specific annealing conditions in a slight excess of sulfur vapor. This interesting reaction mechanism was not thoroughly considered until a recent review by Sopiha et al.⁴ where the importance of BaS3 for the "fast formation" of BaZrS₃ was suggested. Thus, Comparotto et al.²⁴ reported a similarly inspired sulfur-anneal on a cosputtered Ba-Zr film for the formation of $BaZrS_3$ at 590 °C (using a SnS_2 capping layer to prevent oxidation). Wang et al.²³ also reported the synthesis of BaZrS₃ (7 days) at temperatures as low as 450 °C if a small amount of BaS is replaced with BaCl2 though the mechanism for this reaction was unknown. Niu et al.²⁵ also reported the synthesis of BaZrS₃ (and SrZrS₃) from BaS/SrS, Zr, and S at 600 °C with the inclusion of I_2 (60 h—though it is unclear if the reaction happens faster). We note that during the review stage of this work, Vincent et al. 26 reported a liquid fluxassisted growth mechanism for BaZrS3 and BaHfS3 whose results are complementary to that reported herein.

In this work, we address the open question of a low-temperature growth mechanism for BaZrS₃. A systematic study of the reaction conditions (precursor composition, reaction time/temperature, precursor reactivity, and the use of halide catalysts) is reported. Ultimately, we achieve the rapid synthesis of BaZrS₃ via annealing of BaS₃ and ZrS₂ in as little as 5 min at 550 °C. A liquid-assisted grain growth mechanism in molten BaS₃ is responsible for the rapid, low-temperature growth. Alternatively, we demonstrate that the reaction temperature can be further reduced to 500 °C (below the melting point of BaS₃) via the addition of a chloride catalyst, albeit at a slower reaction rate. The reactivity of Zr precursors

decreases successively from ZrS₂, Zr-(S₂Cl₂), ZrS₃, to Zr-metal. The Ba₃Zr₂S₇ phase is obtained with low-reactivity Zr metal, while BaZrS₃ forms with the more reactive precursors. The resulting BaZrS₃ from liquid-assisted grain growth can be purified from residual BaS₃-flux with a water wash. In contrast, Ba₃Zr₂S₇ is found to be unstable in water and converts to the BaZrS₃ phase. The formation conditions for unwanted binaries, such as ZrS₃, BaS₂, and BaS, are discussed. Finally, we extend the liquid-assisted growth mechanism to demonstrate similar results for BaHfS₃, BaNbS₃, and BaTiS₃.

2. RESULTS AND DISCUSSION

2.1. Liquid (BaS₃) Assisted Growth of BaZrS₃. To directly probe the role of BaS₃ in the low-temperature reaction mechanism for BaZrS₃, we first mix ground powders of BaS₃ and ZrS₂ followed by vacuum sealing in a glass ampule. Samples were annealed for 3 h at varying temperatures from 400 to 560 °C. When annealed at lower temperatures (400 and 450 °C), no phase change occurs and the precursor BaS₃ and ZrS₂ powders remain unchanged, as identified in the X-ray diffraction (XRD) data shown in Figure 1a. As the temperature is increased to 500 and 530 $^{\circ}\text{C}\textsc{,}$ several reactions are initiated as evidenced by the XRD (Figure 1a), summarized by (R1)-(R3). [Note that throughout the reactions we refer to $S_{(g,)}$, though gaseous sulfur exists as a polysulfide whose length depends on temperature; $S_{(g.)}$ is shown for clarity in quantifying the amount of sulfur released and required by each reaction.] First, the slow decomposition of BaS₃ into BaS₂ is observed. Second, the complete conversion of ZrS₂ into ZrS₃ is found. As the formation of ZrS₃ requires more sulfur than is released from the partial decomposition of BaS3, we also expect a slow reaction for the formation of BaZrS3, though no BaZrS₃ phase can be easily identified in the XRD (either due the amount formed or poor crystallinity due to the low reaction temperature). The complete conversion of ZrS₂ into ZrS₃ suggests ZrS₃ participates in the slow formation of BaZrS₃ at these temperatures, discussed in more detail when directly using ZrS₃ as a precursor in Section 2.3.

$$BaS_3 \xrightarrow{Slow} BaS_2 + S_{(g.)}$$
 (R1)

$$\operatorname{ZrS}_2 + \operatorname{S}_{(g.)} \xrightarrow{\operatorname{Fast}} \operatorname{ZrS}_3$$
 (R2)

$$BaS_3 + ZrS_3 \xrightarrow{Slow} BaZrS_3 + 3S_{(g.)}$$
 (R3)

When the temperature is increased to 540 $^{\circ}$ C and higher, a dramatic change in the reaction occurs with virtually complete conversion of the precursors into BaZrS₃, with sharp, well-defined peaks in the XRD (Figure 1b). This change occurs close to the reported melting point of BaS₃ at 554 $^{\circ}$ C. ²⁸ To better understand the reaction, BaS₃ was sealed individually in an ampule and annealed. During heating, yellow BaS₃ powder at room temperature gradually turned dark red and eventually into a black liquid droplet above 540 $^{\circ}$ C. This suggests the close relationship between the formation of the BaZrS₃ phase and liquid-phase BaS₃, described by (R4). Trace BaS₃ impurity peaks can also be found for all of the reactions at 540 $^{\circ}$ C and higher.

$$BaS_{3(liq.)} + ZrS_2 \xrightarrow{Fast} BaZrS_3 + 2S_{(g.)}$$
(R4)

To illustrate the fast reaction rate of the $BaS_{3(liq.)}$ growth mechanism in (R4), a series of reactions were performed at 550 °C (to ensure molten BaS_3) for various reaction times. XRD results for this time series are shown in Figure 1c, where phase formation and crystallinity of $BaZrS_3$ are virtually indistinguishable between the 5 min through 3 h reactions (see refined data in the SI).

The formation of BaZrS₃ was further confirmed by Raman spectroscopy, shown in Figure 1d for the same time series. This is primarily verified by the phonon modes for A_g^4 (134.4 cm⁻¹), $(B_{2g}^4 + A_g^5)$ (156.6 cm⁻¹), A_g^6 (215.4 cm⁻¹), and B_{2g}^6 (221.2 cm⁻¹); note that shifts in the reference Raman data reported from Gross et al.¹⁹ (measured at 14 K) are a result of the different measurement temperatures. Strong Raman scattering between 390 and 440 cm⁻¹ is attributed to resonant forbidden LO-phonon scattering in BaZrS₃; ¹⁹ these features appear to broaden and weaken successively for the longer 1 and 3 h annealing times. In addition to BaZrS₃, the residual BaS₃ phase identified in XRD can also be seen in the Raman spectra (454.8 cm⁻¹). Furthermore, trace ZrS₃ (not observed in XRD) is identified by the small peak near 524 cm⁻¹ for the short reaction times, as ZrS₃ reacts slower than ZrS₂ (see Section 2.3).

Here we propose a reactive, liquid-assisted growth mechanism for $BaZrS_3$ in $BaS_{3(liq.)}$ as a flux, as illustrated in Figure 2. Evidence for the liquid-assisted growth mechanism is primarily justified by the rapid crystallization of $BaZrS_3$ in as little as 5 min for temperatures coinciding with that greater

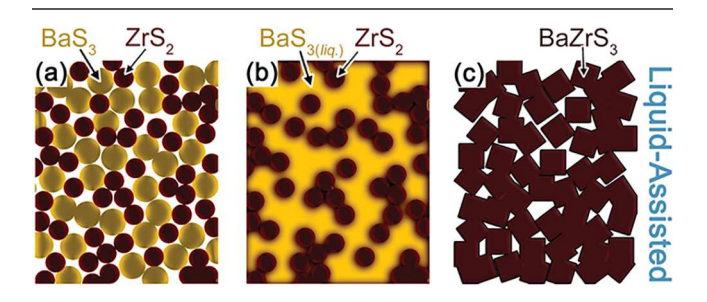


Figure 2. Schematic diagrams for three different stages in the liquid-assisted growth mechanism of $BaZrS_3$. (a) The initial mixture of BaS_3 and ZrS_2 powders at room temperature, (b) the initial formation of BaS_3 liquid at temperatures above ca. 540 °C, and (c) the recovered $BaZrS_3$ product.

than the melting point of BaS₃. The benefits of liquid-assisted growth can be realized through enhanced mass transport to and from grain boundaries and is typically associated with significant grain growth during short processing times at low temperatures (as reported here) relative to solid-state processes.²⁹ The existence of trace BaS₃ is not unexpected since this reactive flux is mixed in stoichiometric proportion. Thus, as the reaction nears completion the continuous distribution of this critical liquid phase disappears, leaving behind isolated pockets of BaS₃. For bulk powder reactions, it may be advantageous to use excess BaS₃ (see (R7)) to maintain a continuous liquid flux throughout the process, as BaS₃ can be readily removed from the final product (see Section 2.2). However, a thin-film geometry may mitigate this issue.

To place our work in context with previously reported syntheses, annealing ZrS2 and BaS is kinetically limited by mass transport during solid-state growth as no liquid flux is present (i.e., high temperatures and long reaction times are required). Alternatively, the inclusion of sulfur vapor during annealing (as in Wang et al.,²³ Comparotto et al.,²⁴ and Turnley et al.²²) allows for the formation of BaS3 from amorphous Ba or BaS precursors—resulting in a similar growth mechanism as identified here at low temperature. Interestingly, if the partial pressure of $S_{(g,)}$ is too high during annealing, the growth of ZrS_3 is increasingly favored relative to the formation of $BaZrS_3$. To avoid this, we propose the direct use of BaS₃ as a barium precursor rather than annealing in excess sulfur vapor; however, excess sulfur vapor released by (R4) is still important to stabilize this reaction, discussed below in Section 2.3. Freund et al.³⁰ recently attempted to fabricate a BaZrS₃ thin film by reacting BaS₃ (from sulfurization of sputtered BaS) with Zr metal; however, this was unsuccessful due to a low annealing temperature (≤460 °C) and the low reactivity of Zr metal as a precursor (see Section 2.3). Finally, the use of oxide precursors is thermodynamically limited, particularly the favorable formation of ZrO2, if any oxygen is present during annealing (i.e., high temperatures and long reaction times are required). This thermodynamic limitation is removed in our work by using oxygen-free precursors.

2.2. Product Purification. To recover a pure BaZrS₃ product, the resulting powders for reactions at 540 °C and higher can be rinsed in H₂O, in which BaS₃ is highly soluble. Accordingly, the product from the 550 °C reaction (3 h) was rinsed 3 times via a dispersion in ultrapure H₂O, which was subsequently recovered with centrifugation. This was followed by a similar ethanol wash 2 times to remove any residual H₂O and vacuum drying at room temperature. During the first round of rinsing in H₂O, the initial blackish powder turned to a dark red precipitate following centrifugation (see inset of Figure 3b for the purified BaZrS₃ powder), while the supernatant turned yellow, indicating the dissolution of BaS₃. Fitted XRD of the recovered pure BaZrS₃ product is shown in Figure 3a (also see Figure S9). Rietveld refinement yields lattice parameters of a = 7.062 Å, b = 9.981 Å, and c = 7.0171Å, which are in good agreement with reported values.³¹ Similarly, the Raman spectrum of the purified powder in Figure 3b indicates the recovery of BaZrS₃.

Photoluminescence (PL), shown in Figure 3c, of the purified BaZrS₃ powder shows an emission peak near 698 nm (1.78 eV) which is in agreement with a range of previously reported values for BaZrS₃, shown by comparison in Figure S10. The PL emission is near the absorption edge measured via diffuse

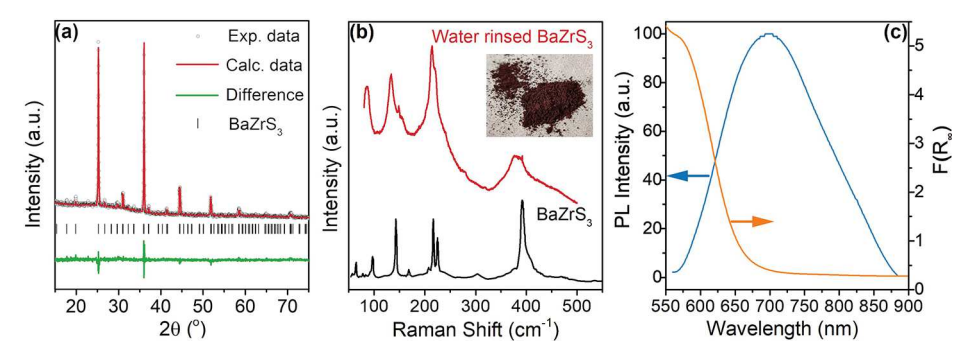


Figure 3. (a) XRD pattern with Rietveld refinement, (b) Raman spectrum, and (c) steady-state PL and absorption spectra for the water-washed BaZrS₃ product from the BaS₃ + ZrS₂ reaction at 550 °C for 3 h. Reference XRD shown in black labeled BaZrS₃ (PDF 01-073-0847). Reference Raman spectrum recorded at 14 K is from Gross et al. ¹⁹

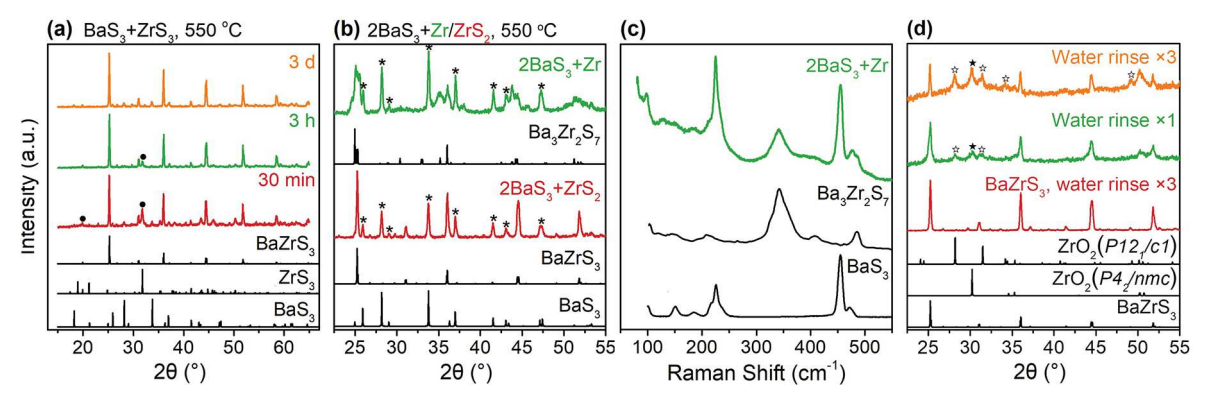


Figure 4. (a) XRD patterns of samples from reaction BaS₃ + ZrS₃ at 550 °C for various reaction times (circles label for ZrS₃). (b) XRD patterns of samples from BaS₃ + Zr-metal (green) and BaS₃ + ZrS₂ (red), both with excess BaS₃ (asterisks label for BaS₃) at 550 °C for 3 h. (c) Raman spectrum of the sample from BaS₃ + Zr-metal with excess BaS₃. Ba₃Zr₂S₇ reference is from Niu et al. BaS₃ reference is measured Raman spectrum of BaS₃ precursor. (d) Powder XRD patterns of water-rinsed samples (orange and green for BaS₃ + Zr-metal and red for BaS₃ + ZrS₂) in (b) (filled stars label for ZrO₂ P4₂/nmc and hollow stars label for ZrO₂ P12₁/c1). Reference XRD patterns are shown in black labeled by compound (BaS₃ PDF 01-073-1177, ZrS₃ PDF 01-080-0926, BaZrS₃ PDF 01-073-0847, ZrO₂ P4₂/nmc PDF 01-079-1763, ZrO₂ P12₁/c1 PDF 01-072-1669).

reflectance (using the Kubelka–Munk transformation), also shown in Figure 3c. We refrain from extracting a band gap value from a Tauc plot of the transformed diffuse reflectance data based on the expected unusual nature of low energy transitions in the electronic structure of BaZrS₃. We expect the optoelectronic properties to be strongly impacted by anionic defects, as similarly reported for A-site alkali earth metal and B-site Group IVB oxide perovskites. 32

2.3. Zr Precursor Reactivity. It has been speculated that ZrS₃ can block the formation of BaZrS₃.⁴ Therefore, variations in the Zr precursor were considered to understand the role of Zr in the reaction pathway. Accordingly, the BaZrS₃ synthesis reaction at 550 °C was repeated for various reaction times; however, ZrS₂ was replaced with ZrS₃. XRD data, shown in Figure 4a, illustrates that BaZrS₃ can also form under these reaction conditions. However, the decreasing presence of ZrS₃ is identified for reactions at both 30 min and 3 h. The virtually complete reaction of ZrS₃ can be observed if the reaction time is extended to 3 days. In all cases, trace BaS₃ is observed, as similarly seen when using ZrS₂ as a precursor. These results illustrate the reduced reactivity of ZrS_3 relative to ZrS_2 in the formation of BaZrS₃, reflected in (R3) and (R4). Accordingly, the use of excess sulfur conditions should be avoided to prevent ZrS₃ formation for the rapid growth of BaZrS₃ at lowtemperature. However, ZrS_3 does not block the growth of BaZrS₃. It can be noted that both Ba in BaS₃ and Zr in ZrS₂ remain in a 12-fold and 6-fold coordination state, respectively,

when transiting to BaZrS₃. In contrast, Zr is in an 8-fold coordination state in ZrS₃; the reduced coordination number of Zr in ZrS₂ may contribute to its increased reactivity.

The reactivity of Zr can be further reduced using elemental Zr-metal as a precursor. The stoichiometric reaction of $BaS_{3(liq.)}$ and Zr at 550 °C (3 h) results in the formation of the (relatively Zr-poor) Ruddlesden—Popper phase $Ba_3Zr_2S_7$ (Figure S11), described by (R5). This is better illustrated when BaS_3 is included in excess, described by (R6), with XRD results shown in Figure 4b (Figure S12). Raman spectroscopy, shown in Figure 4c, further verifies the formation of $Ba_3Zr_2S_7$ in excess BaS_3 . However, when excess BaS_3 is reacted with ZrS_2 rather than Zr-metal, the $BaZrS_3$ phase is still recovered following (R7), with XRD also shown in Figure 4b. Therefore, the formation of the (relatively Zr-poor) $Ba_3Zr_2S_7$ is a result of the reduced Zr reactivity rather than barium excess.

$$4\text{BaS}_{3(liq.)} + 4\text{Zr} \rightarrow \text{Ba}_{3}\text{Zr}_{2}\text{S}_{7} + \text{BaS} + 2\text{ZrS}_{3} + \text{S}_{(g.)}$$
(R5)

$$3BaS_{3(liq.)} + 2Zr \xrightarrow{Excess BaS_3} Ba_3Zr_2S_7 + 2S_{(g.)}$$
 (R6)

$$BaS_{3(liq.)} + ZrS_2 \xrightarrow{Excess BaS_3} BaZrS_3 + 2S_{(g.)}$$
(R7)

The appearance of BaS in (R5) is attributed to the relative reduction in excess sulfur vapor released by the reaction in comparison to (R4), (R6), and (R7). Low-temperature

annealing of BaS_3 in the absence of sulfur vapor results in the decomposition of BaS_3 , as shown in Figure 1a (i.e., sulfur vapor stabilizes the BaS_3 phase). Therefore, a careful consideration of the sulfur vapor pressure is needed for the rapid reaction of pure-phase $BaZrS_3$ at low-temperature, even when elemental sulfur is not included as a precursor. For example, the reactor volume can make a significant contribution to the partial pressure of released $S_{(g)}$.

An attempt was made to purify Ba₃Zr₂S₇ from the excess BaS₃ impurity with the H₂O rinse described in Section 2.2. However, we find Ba₃Zr₂S₇ is not stable in water. Figure 4d shows the XRD for the H₂O-rinsed Ba₃Zr₂S₇ product following 1× and 3× washing steps. In both cases, the Ba₃Zr₂S₇ phase has converted to BaZrS₃. Additionally, the formation of ZrO₂ $(P12_1/c1 \text{ and } P4_2/nmc)$ is observed. The ZrO₂ intensity increases with additional washing steps. Here we attribute the instability of the Ba₃Zr₂S₇ in water due to the intercalation of H₂O into the layered structure (Figure S13). The resulting exfoliated slabs retain a BaZrS3 motif, with any resulting $Ba(OH)_2$ being soluble in the H_2O . The degradation of $BaZrS_3$ slabs into ZrO2 may be a result of their small size, as they originate from an n = 2 Ruddlesden-Popper phase. We similarly find nanoscale BaZrS₃²⁰ is unstable to oxidation, which is also reported for BaZrS3 with relatively reduced crystallinity. 4,33 In contrast, bulk crystalline BaZrS₃ is found to be H₂O-stable here and elsewhere. 18,33

2.4. Vapor-Transport Growth of BaZrS₃ with Cl. The introduction of BaCl₂ into the solid-state syntheses of BaZrS₃ to lower the reaction temperature was first reported by Wang et al.²³ BaZrS₃ could be formed (in addition to BaS₃ and ZrO₂) at 450 °C over 7 days by reacting BaS with ZrS₂ in a specific excess of sulfur vapor, when 10% (molar) of the reactant BaS is replaced with BaCl₂. Little was reported regarding the mechanism of this low temperature synthesis. Similar results have been shown for (non-perovskite) PbTiS₃ and BaTiS₃.³⁴ We have previously shown (Section 2.1) that reaction temperatures lower than 540 °C cannot be used for the rapid reaction of BaS₃ with ZrS₂ into BaZrS₃. However, following Wang et al.,²³ if 10% (molar) BaS₃ is replaced with BaCl₂ we can achieve the formation of BaZrS₃ at 500 °C (3 h), with XRD of the resulting product shown in Figure 5.

In this chloride-containing reaction at 500 °C, liquid BaS₃ is no longer formed due to the low reaction temperature.

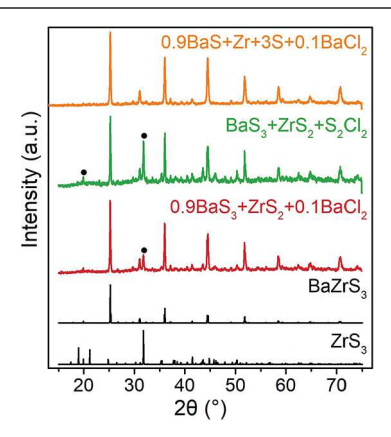


Figure 5. XRD patterns of reactions using Cl at 500 $^{\circ}$ C for 3 h (circles label ZrS₃). Reference XRD patterns are shown in black labeled by compound (ZrS₃ PDF 01-080-0926, BaZrS₃ PDF 01-073-0847.

However, the reaction rate is still relatively rapid as (primarily) BaZrS₃ forms in at least 3 h. Here we speculate a vapor-phase transport mechanism in the presence of chloride. Specifically, S₂Cl₂ can function as the vapor-phase transport agent, as described by (R8). S₂Cl₂ is commonly reported as a vaporphase transport agent for the growth of single crystals, particularly for Group IVB transition metal chalcogenides. 35,30 Furthermore, S₂Cl₂ can form from the reversible reaction of metal chlorides in excess sulfur, 37,38 following (R9). S2Cl2 is a volatile (yellow) liquid at room temperature with a boiling point of 137 °C. Indeed, our work shows the reaction of BaCl₂ + $S_{(g.)}$ (500 °C, 3 h) forms a yellow liquid product when cooled to room temperature (though the instability of S₂Cl₂ in air makes further analysis challenging). Additionally, ZrS₂ can be readily dissolved in S2Cl2 to form a Zr-coordinated compound $Zr-(S_2Cl_2)$. To demonstrate the S_2Cl_2 reaction mechanism, we also directly used S₂Cl₂ in the reaction rather than BaCl2; XRD of the resulting product, Figure 5, shows similar results to the use of BaCl₂.

$$BaS_3 + ZrS_2 + 0.1S_2Cl_{2(g.)} \rightarrow BaZrS_3 + 2.2S_{(g.)}$$
 (R8)

$$BaCl_2 + 3S_{(g.)} \rightarrow S_2Cl_{2(g.)} + BaS$$
 (R9)

In the described chloride reactions, ZrS_3 forms as a secondary phase, following the now competitive reaction (R2), as sulfur is a product in the $BaZrS_3$ reaction (R8). However, a pure-phase $BaZrS_3$ product can be obtained (500 °C, 3 h) by reducing the amount of excess S following (R10); XRD for the product from this reaction is shown in Figure 5. The direct use of BaS_3 is not necessary at this reaction temperature since it occurs below the melting point of BaS_3 , though is expected to form upon reaction with S. Note that in this reaction Zr metal was used, though no Zr_2S_7 phase formed. This indicates a relatively balanced reactivity of Zr_3 and Zr_3S_3 compared to Zr_3S_3 described in Section Zr_3S_3 .

$$0.9 BaS + 0.1 BaCl_{2} + 3S_{(g.)} + Zr$$

$$\rightarrow BaZrS_{3} + 0.1S_{2}Cl_{2} + 0.7S$$
(R10)

These results indicate that $BaCl_2$ acts as a halide source for S_2Cl_2 formation. This is in contrast to speculation that $BaCl_2$ is beneficial to reduce the $S_{(g.)}$ pressure below that required for ZrS_3 formation, or that $BaCl_2$ acts as a precursor for BaS_3 . A proposed schematic for the vapor transport mechanism is depicted in Figure 6 in which accelerated mass transport of Zr via coordination with S_2Cl_2 allows for relatively rapid grain

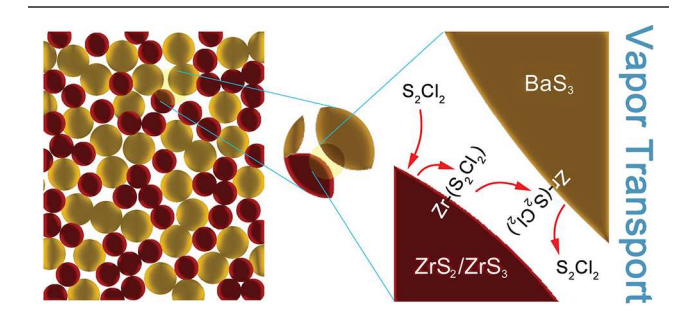


Figure 6. Schematic diagram of the vapor-transport growth mechanism. ZrS_2/ZrS_3 is shown in red and BaS_3 in yellow. A $Zr-(S_2Cl_2)$ vapor-transport process is illustrated.

growth of BaZrS $_3$ (compared to the absence of S $_2$ Cl $_2$ in which BaZrS $_3$ growth is limited for temperatures <540 °C).

2.5. Application of BaS₃-Flux for Additional ABS₃ Chalcogenides. Following the liquid-assisted growth mechanism described here-in (Section 2.1), BaS_{3(liq.)} can similarly react with HfS₂, NbS₂, and TiS₂ at 550 °C (3 h) to readily form (chalcogenide perovskite) BaHfS₃, (hexagonal) BaNbS₃, and (hexagonal) BaTiS₃, respectively. XRD data are shown in Figure 7 following the water wash described in Section 2.2 (to

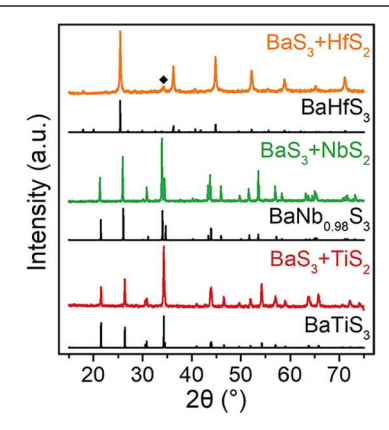


Figure 7. XRD patterns of samples from reaction of $(BaS_3 + HfS_2)$, $(BaS_3 + NbS_2)$, and $(BaS_3 + TiS_2)$ at 550 °C for 3 h (diamond labels an unknown impurity peak in the BaHfS₃ product). Reference XRD patterns are shown in black labeled by compound $(BaTiS_3 \text{ PDF 01-071-2000}, BaNb_{0.98}S_3 \text{ PDF 01-083-0359}, and BaHfS₃ from Lelieveld et al.³¹).$

remove residual BaS₃). Diffuse reflectance data for BaHfS₃ (Figure S16) show a shift to higher energy compared to BaZrS₃, which is in agreement with its higher bandgap.³⁹ Images of the resulting powders as well as Rietveld refinement results can be found in the SI.

3. CONCLUSIONS

In this work, a low-temperature, liquid-assisted growth mechanism is demonstrated for Ba-based chalcogenide perovskites and related chalcogenides, including BaZrS₃, Ba₃Zr₂S₇, BaHfS₃, BaNbS₃, and BaTiS₃. The importance of liquid-BaS₃ is demonstrated for the rapid growth of these materials in as little as 5 min at temperature ≥540 °C. The reactivity of Zr is found to decrease from ZrS₂, Zr-(S₂Cl₂), to ZrS₃, ultimately resulting in the formation of the (relatively Zr-poor) Ruddlesden-Popper Ba₃Zr₂S₇ phase in the limit of elemental Zr-metal as a precursor. In this growth mechanism, we further demonstrate the role of $S_{(g.)}$ in the undesirable formation of ZrS_3 and in the stabilization of the desirable BaS₃ phase. The resulting BaZrS₃ from liquid-assisted grain growth can be purified from residual BaS₃-flux with a straightforward water wash. In contrast, Ba₃Zr₂S₇ is found to be unstable in water and converts to the BaZrS₃ phase, which oxidizes easily in water due to its small size. Lastly, in the absence of a liquid-phase, we also demonstrate a vapor-transport growth mechanism using S₂Cl₂ for the formation of BaZrS₃ at temperatures as low as 500 °C in at least 3 h.

BaZrS₃ is predicted to be thermodynamically stable relative to secondary binary phases, with the distorted perovskite phase as the ground state.⁴ Our results support this conclusion. Although ZrS₃ forms in excess S_(g,), it will react to form BaZrS₃ given enough time (kinetically limited). On the other hand, it

has been proposed that $BaZrS_3$ may be unstable at $S_{(g.)}$ pressures where ZrS_3 forms; we find that this is not the case for similar reasons. In contrast, at low $S_{(g.)}$ pressures, the reaction is kinetically limited by diffusion in the absence of liquid- BaS_3 .

These results demonstrate the feasibility of scalable processing for the formation of chalcogenide perovskite thinfilms at suitable temperatures, and several approaches to their formation and purification are shown.

4. EXPERIMENTAL METHODS

4.1. Materials. Sulfuric acid $(H_2SO_4, 6.0 \text{ N}, \text{ cat. No. } 8330\text{-}16)$, barium chloride $(BaCl_2, \geq 97\%, \text{ cat. No. } B31\text{-}500)$, elemental sulfur (S, 99.50%, cat. No. AA1078536), titanium powder (Ti, 99.5% metals basis, cat. No. AA4310522), zirconium powder (Zr, cat. No. AA0041814), and hafnium powder (Hf, 99.6% metals basis excluding Zr, cat. No. AA1020106) were purchased from Fisher Scientific. Sulfur monochloride $(S_2Cl_2, 98\%, \text{ cat. No. } 157759)$ was purchased from Sigma-Aldrich. Sulfur and zirconium powder were dried in a vacuum oven at 75 °C for 2 days before use. All other materials were used as received.

4.2. Precursor Synthesis. BaS₃. First, Ba(OH)₂·8H₂O (32.546 g, 100 mmol) was dispersed in 200 mL of H₂O. The 6.0 N H₂SO₄ (33.3 mL, 100 mmol) was added slowly into the dispersion with vigorous agitation and an ice bath. The reaction was stopped at 5 h, and BaSO₄ was recovered by centrifugation. The product was washed with H₂O three more times before drying in the oven at 110 °C overnight. BaS was prepared by reduction of BaSO₄ with 4% hydrogen-balanced Ar in a tube furnace at 1000 °C for 12 h. The BaS product was a white powder. It was immediately taken into a N2-filled glovebox and ground into fine white powder. BaS (5698 mg, 33.64 mmol) and elemental sulfur (2157 mg, 67.28 mmol) were mixed by grinding with an agate mortar and pestle in the glovebox. The mixture was then loaded into a dried borosilicate glass tube (OD 0.748 in, ID 0.606 in, length ca. 16 in) and flame-sealed under vacuum forming an ampule (length ca. 12 in). The ampule was heated in a muffle furnace from room temperature to 400 °C, with a ramp rate of 5 °C/min, and maintained for 12 h. The furnace was then turned off and allowed to slowly cool down to room temperature. The initial white BaS powder turned to lemon-yellow BaS3 and was stored in the glovebox. Caution should be used when working with BaS3 as barium polysulfides are water-soluble and known to be toxic upon ingestion, or can be an irritant upon skin exposure.

ZrS₂ and ZrS₃. Following the same mixing, evacuation, and sealing procedure of BaS3 preparation, ZrS3 was first made by reacting dried zirconium powder (Zr, 1095 mg, 12 mmol) and elemental sulfur (1154 mg, 36 mmol) in a dried borosilicate ampule (OD 0.748 in., ID 0.606 in., length ca. 12 in.). The mixture was heated in a muffle furnace to 300 °C, at 5 °C/min ramp rate, and maintained for 6 h. Next, it was heated in the same fashion to 400 °C, then 500 °C, at which point it was maintained 15 more hours. The furnace was then turned off and allowed to slowly cool down to room temperature. The initial dark gray mixture turned to a red powder of ZrS3. For ZrS2 the ZrS₃ powder was further decomposed in a tube furnace under ultrapure Ar. The tube furnace containing ZrS3 was increased to 100 °C and maintained there for 30 min. The temperature was then increased to 800 °C within 1 h and maintained there for 2 h. The furnace was then turned off and allowed to slowly cool down to room temperature. The product ZrS2 was a dark red powder and was stored in the glovebox.

 HfS_2 . Following the same mixing, evacuation, and sealing procedure of BaS₃ preparation, hafnium powder (1000 mg, 5.60 mmol) was mixed with elemental sulfur (359.2 mg, 11.20 mmol) into a dried quartz ampule (OD 0.55 in., ID 0.39 in., length ca. 13 in.). The mixture was heated in a muffle furnace to 750 °C from room temperature, at a 5 °C/min ramp rate, and maintained for 12 h. The furnace was then turned off and allowed to slowly cool down to room

temperature. A dark red/brown HfS_2 product formed and was stored in the glovebox.

 TiS_2 . Following the same mixing, evacuation, and sealing procedure of BaS₃ preparation, TiS₃ was first made by reacting Ti powder (1107 mg, 23.10 mmol) and elemental sulfur (2222 mg, 69.30 mmol) into a dried borosilicate ampule (OD 0.748 in., ID 0.606 in., length ca. 12 in.). Heating and cooling followed the procedure described for ZrS₃. The TiS₃ was then decomposed into TiS₂ in the same way as ZrS₂, though for 1.5 h instead of 2 h. The final product was greenish-yellow TiS₂ powder and was stored in the glovebox.

 NbS_2 . Following the same mixing, evacuation, and sealing procedure of BaS_3 preparation, niobium powder (591.6 mg, 6.37 mmol) was mixed with elemental sulfur (408.3 mg, 12.74 mmol) into a dried quartz ampule (OD 0.55 in., ID 0.39 in., length ca. 13 in.). The mixture was heated in a muffle furnace to 850 °C from room temperature, at 5 °C/min, and maintained for 12 h. The furnace was then turned off and allowed to slowly cool down to room temperature. A black NbS_2 product formed and was stored in the glovebox.

4.3. Ternary ABS₃ and A₃B₂S₇ Chalcogenides. In a typical reaction, 1.5 mmol fine powder of both A site source precursor (BaS or BaS₃) and B site source precursor (ZrS₂, ZrS₃, Zr-metal powder, HfS₂, NbS₂, TiS₂) were measured in the glovebox and ground together with an agate mortar and pestle. The mixture was subsequently transferred into a borosilicate glass tube (OD 0.5 in., ID 0.38 in., length ca. 6 in.) and flame-sealed under vacuum forming an ampule (ca. 3 in long). The ampule was transferred into a preheated muffle furnace at the desired temperature (560 °C, 550 °C, 540 °C, 530 °C, 500 °C, 450 °C, 400 °C) for different times (3 h, 1 h, 30 min, 5 min). The ampule was taken directly out of the furnace and cooled in air at the end of the reaction. For BaS3 excess and chlorideinvolved reactions, the Zr precursor remained 1.5 mmol, and BaS3 was adjusted accordingly. For the S_2Cl_2 -involved reaction, S_2Cl_2 (12 μ L) was first added to the end-sealed tube, followed by the addition of a stoichiometric mixture of BaS3 and ZrS2 on top. Extra caution should be used when working with corrosive S_2Cl_2 . It is highly sensitive to water/moisture and hydrolyzes to release HCl mist and SO₂.

4.4. Ampule Sealing. Prior to sealing, all ampules were closed with a stopcock in the inert N_2 environment in the glovebox. Next, the closed tubes were taken out of the glovebox and directly attached to a roughing pump under vacuum for 10 min (S_2Cl_2 reactions were only pumped for 1 min). The ampules were then flame-sealed under vacuum (ca. 100-200 mTorr base pressure). Borosilicate tubes were sealed using a methylacetylene-propadiene propane (MAPP) torch while quartz tubes were sealed using an acetylene torch.

In the sulfurization reactions, sulfur quantities were as follows: (1) 38.0 mg/cm³ for BaS into BaS₃, (2) 20.3 mg/cm³ for Zr into ZrS₃, and (3) 19.5 mg/cm³ for Ti into TiS₃, using borosilicate glass ampules with a 1.8 mm wall thickness. For the sulfurization reactions of (1) Hf into HfS₂ and (2) Nb into NbS₂, 14.1 mg/cm³ and 16.0 mg/cm³ of sulfur were used, respectively, with quartz glass ampules of 2.0 mm wall thickness. Although no elemental sulfur was used for ABX₃ syntheses, the sulfur generated in the reactions is estimated to be ca. 17.3 mg/cm³ in borosilicate ampules with a 1.5 mm wall thickness by the end of the reactions. Under the conditions described, no ampule cracking was experienced. However, deviations from these values (e.g., increased sulfur amount, thinner wall thickness, or faster heating ramp rate) might increase the risk of pressure build-up and consequent ampule cracking.

4.5. Measurements. XRD measurements were performed with a PANalytical XPert Powder diffractometer using Cu K α radiation at 45 kV and 40 mA and a zero-background holder. For the purified BaZrS $_3$, the XRD sample is a dropcast film. For all the other samples, powders were used for XRD measurements. Photoluminescence (PL), diffuse reflectance, and Raman measurements were performed on powder samples. PL was performed at 532 nm excitation. Diffuse reflectance measurements were performed with a white lamp and 99.9% diffuse reflectance standard. Both measurements utilized a NIREOS GEMINI interferometer and PicoQuant TimeHarp 260 time-correlated single photon counting system in "T2" mode to record interferograms, from

which PL or reflectance spectra were reconstructed by fast Fourier transform. Raman spectroscopy for water rinsed BaZrS₃ and 2BaS₃ + Zr-metal reaction was performed on a Horiba LabRAM ARAMIS with 785 nm wavelength excitation and a 10× objective. Raman spectra of the other samples were recorded using a Renishaw inVia Reflex Raman Microscope in a backscattering geometry with different excitation wavelengths including 785, 633, and 532 nm with a 50× objective. The measurement spot of each probed sample has been visually checked before and after measurement, indicating no laser damage. Furthermore, each laser has been calibrated by using a Si wafer.

ASSOCIATED CONTENT

Solution Supporting Information

The Supporting Information is available free of charge at https://pubs.acs.org/doi/10.1021/acs.chemmater.3c00494.

Additional XRD of precursors, $BaZrS_3$, and $Ba_3Zr_2S_7$, Rietveld refinement for XRD presented here-in, comparison of PL data for $BaZrS_3$, intercalation schematic for $Ba_3Zr_2S_7$, and diffuse reflectance data for $BaHfS_3$ (PDF)

AUTHOR INFORMATION

Corresponding Author

Charles J. Hages – Department of Chemical Engineering, University of Florida, Gainesville, Florida 32611, United States; orcid.org/0000-0003-4054-1218;

Email: c.hages@ufl.edu

Authors

Ruiquan Yang — Department of Chemical Engineering, University of Florida, Gainesville, Florida 32611, United States

Jessica Nelson — Department of Chemical Engineering, University of Florida, Gainesville, Florida 32611, United States

Calvin Fai — Department of Chemical Engineering, University of Florida, Gainesville, Florida 32611, United States;
orcid.org/0000-0001-8866-3674

Hasan Arif Yetkin – Department of Physics and Materials Science, University of Luxembourg, L-4422 Belvaux, Luxembourg

Chase Werner — Department of Chemical Engineering, University of Florida, Gainesville, Florida 32611, United States

Merielle Tervil – Department of Chemical Engineering, University of Florida, Gainesville, Florida 32611, United States

Alexander D. Jess — Department of Chemical Engineering, University of Florida, Gainesville, Florida 32611, United States

Phillip J. Dale – Department of Physics and Materials Science, University of Luxembourg, L-4422 Belvaux, Luxembourg

Complete contact information is available at: https://pubs.acs.org/10.1021/acs.chemmater.3c00494

Notes

The authors declare no competing financial interest.

ACKNOWLEDGMENTS

C.J.H. acknowledges financial support from the SSMC program at the National Science Foundation (DMR-

2044859). H.A.Y. acknowledges financial support from University of Luxembourg.

REFERENCES

- (1) Niu, S.; Milam-Guerrero, J.; Zhou, Y.; Ye, K.; Zhao, B.; Melot, B. C.; Ravichandran, J. Thermal stability study of transition metal perovskite sulfides. *J. Mater. Res.* **2018**, *33*, 4135–4143.
- (2) Perera, S.; Hui, H.; Zhao, C.; Xue, H.; Sun, F.; Deng, C.; Gross, N.; Milleville, C.; Xu, X.; Watson, D. F.; Weinstein, B.; Sun, Y.-Y.; Zhang, S.; Zeng, H. Chalcogenide perovskites an emerging class of ionic semiconductors. *Nano Energy* **2016**, *22*, 129–135.
- (3) Swarnkar, A.; Mir, W. J.; Chakraborty, R.; Jagadeeswararao, M.; Sheikh, T.; Nag, A. Are Chalcogenide Perovskites an Emerging Class of Semiconductors for Optoelectronic Properties and Solar Cell? *Chem. Mater.* **2019**, *31*, 565–575.
- (4) Sopiha, K. V.; Comparotto, C.; Márquez, J. A.; Scragg, J. J. S. Chalcogenide Perovskites: Tantalizing Prospects, Challenging Materials. *Advanced Optical Materials* **2022**, *10*, 2101704.
- (5) Buffiere, M.; Dhawale, D. S.; El-Mellouhi, F. Chalcogenide Materials and Derivatives for Photovoltaic Applications. *Energy Technology* **2019**, *7*, 1900819.
- (6) Jaramillo, R.; Ravichandran, J. In praise and in search of highly-polarizable semiconductors: Technological promise and discovery strategies. *APL Materials* **2019**, *7*, 100902.
- (7) Nishigaki, Y.; Nagai, T.; Nishiwaki, M.; Aizawa, T.; Kozawa, M.; Hanzawa, K.; Kato, Y.; Sai, H.; Hiramatsu, H.; Hosono, H.; Fujiwara, H. Extraordinary Strong Band-Edge Absorption in Distorted Chalcogenide Perovskites. *Solar RRL* **2020**, *4*, 1900555.
- (8) Wu, X.; Gao, W.; Chai, J.; Ming, C.; Chen, M.; Zeng, H.; Zhang, P.; Zhang, S.; Sun, Y. Y. Defect tolerance in chalcogenide perovskite photovoltaic material BaZrS₃. *Science China Materials* **2021**, *64*, 2976–2986.
- (9) Meng, W.; Saparov, B.; Hong, F.; Wang, J.; Mitzi, D. B.; Yan, Y. Alloying and Defect Control within Chalcogenide Perovskites for Optimized Photovoltaic Application. *Chem. Mater.* **2016**, 28, 821–829.
- (10) Hahn, H.; Mutschke, U. Untersuchungen über ternäre Chalkogenide. XI. Versuche zur Darstellung von Thioperowskiten. Zeitschrift fur anorganische und allgemeine Chemie 1957, 288, 269–278.
- (11) Clearfield, A. The synthesis and crystal structures of some alkaline earth titanium and zirconium sulfides. *Acta Crystallogr.* **1963**, *16*, 135–142.
- (12) Márquez, J. A.; Rusu, M.; Hempel, H.; Ahmet, I. Y.; Kölbach, M.; Simsek, I.; Choubrac, L.; Gurieva, G.; Gunder, R.; Schorr, S.; Unold, T. BaZrS₃ Chalcogenide Perovskite Thin Films by H₂S Sulfurization of Oxide Precursors. *J. Phys. Chem. Lett.* **2021**, *12*, 2148–2153.
- (13) Wei, X.; et al. Realization of BaZrS₃ chalcogenide perovskite thin films for optoelectronics. *Nano Energy* **2020**, *68*, 104317.
- (14) Yu, Z.; Wei, X.; Zheng, Y.; Hui, H.; Bian, M.; Dhole, S.; Seo, J. H.; Sun, Y. Y.; Jia, Q.; Zhang, S.; Yang, S.; Zeng, H. Chalcogenide perovskite BaZrS₃ thin-film electronic and optoelectronic devices by low temperature processing. *Nano Energy* **2021**, *85*, 105959.
- (15) Surendran, M.; Chen, H.; Zhao, B.; Thind, A. S.; Singh, S.; Orvis, T.; Zhao, H.; Han, J.-K.; Htoon, H.; Kawasaki, M.; Mishra, R.; Ravichandran, J. Epitaxial thin films of a chalcogenide perovskite. *Chem. Mater.* **2021**, *33*, 7457–7464.
- (16) Comparotto, C.; Davydova, A.; Ericson, T.; Riekehr, L.; Moro, M. V.; Kubart, T.; Scragg, J. Chalcogenide Perovskite BaZrS₃: Thin Film Growth by Sputtering and Rapid Thermal Processing. *ACS Applied Energy Materials* **2020**, *3*, 2762–2770.
- (17) Sadeghi, I.; Ye, K.; Xu, M.; Li, Y.; LeBeau, J. M.; Jaramillo, R. Making BaZrS₃ Chalcogenide Perovskite Thin Films by Molecular Beam Epitaxy. *Adv. Funct. Mater.* **2021**, *31*, 2105563.
- (18) Gupta, T.; et al. An Environmentally Stable and Lead-Free Chalcogenide Perovskite. *Adv. Funct. Mater.* **2020**, *30*, 2001387.
- (19) Gross, N.; Sun, Y.-Y.; Perera, S.; Hui, H.; Wei, X.; Zhang, S.; Zeng, H.; Weinstein, B. Stability and band-gap tuning of the

- chalcogenide perovskite BaZrS₃ in Raman and optical investigations at high pressures. *Physical Review Applied* **2017**, *8*, 044014.
- (20) Yang, R.; Jess, A. D.; Fai, C.; Hages, C. J. Low-Temperature, Solution-Based Synthesis of Luminescent Chalcogenide Perovskite BaZrS₃ Nanoparticles. *J. Am. Chem. Soc.* **2022**, *144*, 15928–15931.
- (21) Zilevu, D.; Parks, O. O.; Creutz, S. E. Solution-phase synthesis of the chalcogenide perovskite barium zirconium sulfide as colloidal nanomaterials. *Chem. Commun.* **2022**, *58*, 10512–10515.
- (22) Turnley, J. W.; Vincent, K. C.; Pradhan, A. A.; Panicker, I.; Swope, R.; Uible, M. C.; Bart, S. C.; Agrawal, R. Solution Deposition for Chalcogenide Perovskites: A Low-Temperature Route to BaMS₃ Materials (M = Ti, Zr, Hf). *J. Am. Chem. Soc.* **2022**, *144*, 18234–18239.
- (23) Wang, Y.; Sato, N.; Yamada, K.; Fujino, T. Synthesis of BaZrS₃ in the presence of excess sulfur. *J. Alloys Compd.* **2000**, 311, 214–223.
- (24) Comparotto, C.; Ström, P.; Donzel-Gargand, O.; Kubart, T.; Scragg, J. J. Synthesis of BaZrS₃ Perovskite Thin Films at a Moderate Temperature on Conductive Substrates. *ACS Applied Energy Materials* **2022**, *5*, 6335–6343.
- (25) Niu, S.; Huyan, H.; Liu, Y.; Yeung, M.; Ye, K.; Blankemeier, L.; Orvis, T.; Sarkar, D.; Singh, D. J.; Kapadia, R.; Ravichandran, J. Bandgap Control via Structural and Chemical Tuning of Transition Metal Perovskite Chalcogenides. *Adv. Mater.* **2017**, *29*, 1604733.
- (26) Vincent, K. C.; Agarwal, S.; Turnley, J. W.; Agrawal, R. Liquid Flux—Assisted Mechanism for Modest Temperature Synthesis of Large-Grain BaZrS3 and BaHfS3 Chalcogenide Perovskites. *Advanced Energy and Sustainability Research* **2023**, *4*, 2300010.
- (27) v. Schnering, H. G.; Goh, N. K. Die Strukturen der Polysulfide BaS₃, SrS₃, BaS₂ und SrS₂. Die Naturwissenschaften **1974**, 61, 272.
- (28) Lide, D. R., Ed. CRC Handbook of Chemistry and Physics, 73rd ed.; CRC Press: 1992; pp 4-43.
- (29) Hages, C. J.; Koeper, M. J.; Miskin, C. K.; Brew, K. W.; Agrawal, R. Controlled Grain Growth for High Performance Nanoparticle-Based Kesterite Solar Cells. *Chem. Mater.* **2016**, 28, 7703–7714.
- (30) Freund, T.; Cicconi, M. R.; Wellmann, P. J. Fabrication of Bariumtrisulphide Thin Films as Precursors for Chalcogenide Perovskites. *Physica Status Solidi B* **2022**, 259, 2200094.
- (31) Lelieveld, R.; IJdo, D. J. W. Sulphides with the GdFeO3 structure. Acta Crystallographica Section B Structural Crystallography and Crystal Chemistry 1980, 36, 2223–2226.
- (32) Tufte, O. N.; Chapman, P. W. Electron Mobility in Semiconducting Strontium Titanate. *Phys. Rev.* **1967**, *155*, 796–802.
- (33) Wang, Y.; Sato, N.; Fujino, T. Synthesis of BaZrS₃ by short time reaction at lower temperatures. *J. Alloys Compd.* **2001**, 327, 104–112.
- (34) Wang, Y.; Sato, N.; Yamada, K.; Fujino, T. Effect of Halide Addition on the Syntheses of PbTiS₃ and Ba_xTiS_y in Sulfur Melt. Shigen-to-Sozai **2000**, 116, 703–710.
- (35) Lévy, F.; Berger, H. Single crystals of transition metal trichalcogenides. *J. Cryst. Growth* **1983**, *61*, 61–68.
- (36) Binnewies, M.; Glaum, R.; Schmidt, M.; Schmidt, P. Chemical Vapor Transport Reactions; De Gruyter: 2012; Chapter 7, pp 321–402.
- (37) Kleinert, P.; Funke, A. Über Reaktionen von Magnesiumferrit und Magnetit mit Dischwefeldichlorid. *Die Naturwissenschaften* **1960**, 47, 106–107.
- (38) Engelke, F.; Zare, R. Crossed-beam chemiluminescence: The alkaline earth rearrangement reaction $M + S_2Cl_2 \rightarrow S_2^* + MCl_2$. Chem. Phys. 1977, 19, 327–340.
- (39) Sun, Y.; Agiorgousis, M. L.; Zhang, P.; Zhang, S. Chalcogenide perovskites for photovoltaics. *Nano Lett.* **2015**, *15*, 581–585.